E-ISSN : 2541-5794
P-ISSN : 2503-216X

Journal of Geoscience,
Engineering, Environment, and Technology
Vol xx No xx 20xx

RESEARCH ARTICLE

# Hydrothermal Alteration and Geochemical Signatures of High-Sulfidation Epithermal Gold Mineralization in Petai Patah, West Kalimantan, Indonesia

Noprizan Azmi [1], Arie Naftali Hawu Hede[2,*], Syafrizal[2]

[1] *Master Program of Mining Engineering, Faculty of Mining and Petroleum Engineering, Institut Teknologi Bandung, Indonesia 40132*
[2] *Earth Resources Exploration Research Group, Faculty of Mining and Petroleum Engineering, Institut Teknologi Bandung, Indonesia 40132*

* Corresponding author : ariehede@itb.ac.id
Tel.:+62-22-2502239; fax: +62-22-2504209
Received: Oct 1, 2016; Accepted: Nov 20, 2016.
DOI: 10.24273/jgeet.2016.1.2.001

**Abstract**

High-sulfidation epithermal systems are an important source of precious metals in volcanic-arc settings, yet detailed studies of these systems in the Schwaner Mountains of western Borneo remain scarce. This study investigates the hydrothermal alteration and geochemical signatures of high-sulfidation epithermal gold mineralization in the Petai Patah area, Ketapang District, West Kalimantan, Indonesia, hosted within the Cretaceous Sukadana Granite and the Paleogene Kerabai Volcanic Complex. An integrated analytical approach was employed, combining reflectance spectroscopy, petrographic analysis, X-ray diffraction (XRD), and whole-rock geochemistry on 15 representative rock samples from surface outcrops and drill cores. Results reveal a well-defined hydrothermal alteration zonation, comprising an advanced argillic core (alunite, pyrophyllite, dickite) in Pit Lokma, surrounded by a phyllic zone (dominant muscovite/sericite–illite–pyrite assemblage) extending into Pit Limun. Gold mineralization (maximum 1.61 ppm Au in sample DC 347, Pit Limun) is spatially correlated with these alteration zones and occurs in association with sulfide minerals, suggesting a structurally controlled fluid pathway. Elevated As concentrations in gold-bearing samples from Pit Limun, together with the diagnostic mineralogical assemblage, support the interpretation of a high-sulfidation epithermal system. This study provides new insights into the spatial relationship between alteration zonation and gold enrichment within a high-sulfidation epithermal system, offering implications for mineral exploration in similar magmatic arc settings across Southeast Asia.

**Keywords:** Epithermal gold deposit; High-sulfidation system; Hydrothermal alteration; Reflectance spectroscopy; Geochemistry; West Kalimantan



## 1. Introduction

Indonesia, located at the convergence of the Eurasian, Indo-Australian, and Pacific tectonic plates, hosts an extensive array of magmatic arcs and associated hydrothermal mineral systems. This geodynamic setting provides favorable conditions for the formation of economically significant mineral deposits, including porphyry copper and epithermal gold systems (Carlile and Mitchell, 1994; Ernawati et al., 2019; Hall, 2002; Idrus et al., 2021; Syafrizal et al., 2017) and metamorphic-hosted orogenic gold (Hasria et al., 2019; Idrus et al., 2017). Among these, epithermal deposits constitute a key source of gold (Au) and silver (Ag), commonly hosted in volcanic arcs and formed at shallow crustal levels (50–1500 m depth) under moderate temperatures (150–300 °C) (Angeles et al., 2002; Sillitoe and Hedenquist, 2003).

Epithermal systems are broadly classified into high-sulfidation (HS) and low-sulfidation (LS) types, based on the oxidation state and chemistry of the hydrothermal fluids (Sillitoe and Hedenquist, 2003). High-sulfidation systems are typically associated with acidic, magmatic-derived fluids and are characterized by intense leaching, advanced argillic alteration, and an assemblage of sulfide and sulfosalt minerals (Gemmell, 2007; White and Hedenquist, 1995). These deposits often occur in association with volcanic complexes and shallow intrusions (Gemmell, 2007; Prihatmoko and Idrus, 2020; Sillitoe, 2010), making them important exploration targets in arc-related settings.

In West Kalimantan, historical and contemporary gold mining activities have indicated the presence of epithermal-style mineralization (Ilmawan et al., 2023; Williams et al., 1986, 1988). However, scientific studies integrating modern alteration mapping techniques and geochemical analyses remain limited. The Petai Patah area, situated within the Sukadana Granite and Kerabai Volcanic Complex, lies along a tectonically active corridor known to host multiple hydrothermal systems. Despite ongoing mining and exploration activities, detailed studies on the spatial distribution of hydrothermal alteration zones and their geochemical relationship with gold mineralization in this area are scarce.

This study addresses this gap by characterizing the hydrothermal alteration and gold mineralization patterns at the Limun and Lokma Pits in Petai Patah. We employ an integrated approach that combines reflectance spectroscopy, petrography, X-ray diffraction (XRD), and geochemical analysis (X-ray fluorescence/XRF, atomic absorption spectroscopy/AAS, and inductively coupled plasma-mass spectroscopy/ICP-MS) to delineate alteration zones and their relationship to gold

enrichment. The objectives are to: (i) characterize the alteration mineral assemblages and their spatial distribution, (ii) evaluate geochemical signatures associated with gold mineralization, and (iii) interpret the genetic model and structural controls of the system. The results provide new insights into high-sulfidation epithermal systems in the magmatic arc setting of western Borneo and may serve as a reference for similar mineral exploration efforts in Southeast Asia.

## 2. Geological Setting

The Petai Patah area, located in the Ketapang Regency of West Kalimantan, is situated within the Southwest Borneo Block—an accreted continental terrane that amalgamated with Sundaland during the Late Cretaceous to Early Cenozoic (Hall, 2012). The region underwent extensive Cretaceous subduction-related magmatism, resulting in the formation of the Schwaner Mountains Magmatic Arc. This arc is characterized by voluminous granitoid intrusions, including the Sukadana Batholith, which plays a critical role in the metallogenic framework of the area (Hall and Nichols, 2002; Williams et al., 1988).

The local geology is dominated by two principal lithological units: the Cretaceous Sukadana Granite and the overlying Paleogene volcanic rocks of the Kerabai Volcanic Complex (Fig. 1a) (Rustandi and De Keyser, 1993). The Sukadana Granite is a coarse-grained, biotite-hornblende-bearing granodiorite to granite with a hypidiomorphic texture, composed primarily of plagioclase, quartz, K-feldspar, and minor accessory minerals such as zircon and magnetite. This intrusive suite serves as both the thermal engine and a potential source of metal for the hydrothermal system.

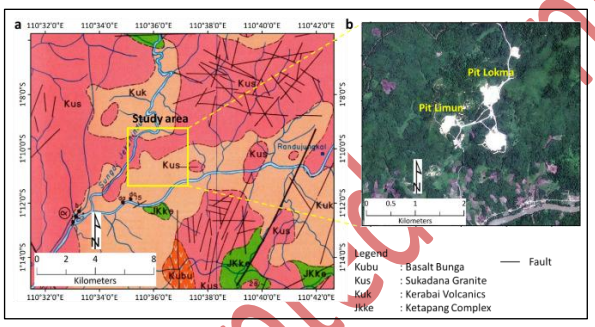


Fig. 1. (a) Regional geological map of the study area showing the distribution of lithologies, including the Sukadana Granite (Kus) and surrounding volcanic units, with the study area outlined in yellow (modified from Rustandi and De Keyser, 1993). (b) Situational map of Pit Lokma and Pit Limun within the study area, overlaid on true-color PlanetScope Basemap (@Planetscope) satellite imagery acquired in September 2024.

Unconformably overlying the granite are andesitic to dacitic lava flows, volcanic breccias, and tuffs of the Kerabai Complex. These volcanic rocks exhibit heterogeneity in composition and texture, and are variably fractured, making them highly permeable and suitable as host rocks for epithermal mineralization. The contact between the granitoids and volcanic rocks is often obscured by hydrothermal brecciation and pervasive alteration.

A conjugate system of NW structurally controls the mineralized zones at Pit Limun and Pit Lokma–SE and NE–SW-trending faults (Rustandi and De Keyser, 1993). While large-scale fault planes are not directly exposed, the alignment of breccia bodies, quartz-sulfide veins, and alteration zones suggests the presence of major subsurface structures that channeled hydrothermal fluids (Hedenquist et al., 2000; Heriawan et al., 2022). The most intense alteration and highest Au grades are consistently observed near these interpreted structural intersections.

The stratigraphy in the study area is simplified into three informal units: (1) the granitoid basement of the Sukadana Batholith, (2) the overlying volcanic sequence of the Kerabai Complex, and (3) late-stage hydrothermal breccias and vein networks. The spatial relationship among these units and their structural juxtaposition have played a crucial role in the development and localization of the high-sulfidation epithermal system identified in this study.

## 3. Materials and Methods

This study was conducted at two mineralized sites; Pit Limun and Pit Lokma, in the Petai Patah area of Ketapang Regency, West Kalimantan (Fig. 1b). Geological fieldwork involved detailed mapping and systematic sampling aimed at characterizing hydrothermal alteration patterns and their geochemical association with gold mineralization. A total of 15 representative rock samples were collected, comprising 9 samples from surface outcrops and 6 samples from diamond drill core. The drill core samples were obtained from the coreshed of PT Serinding Sumber Makmur (PT SSM), the mining company operating in the area. Sampling locations were selected to represent different lithologies, alteration intensities, and spatial relationships to structural features. The complete sample inventory and analytical methods applied to each sample are presented in Table 1.

Table 1. Sample list and analytical methods applied in this study

| Sample ID | Pit | Type | Analyses |
|---|---|---|---|
| WS 01 | Limun | Outcrop | Spec, XRD, XRF |
| WS 02 | Limun | Outcrop | Spec, Petro |
| WS 03 | Limun | Outcrop | Spec, AAS |
| WS 04 | Limun | Outcrop | Spec, XRD, XRF, AAS, Petro |
| WS 05 | Limun | Outcrop | Spec |
| WS 06 | Limun | Outcrop | Spec, XRF |
| WS 07 | Lokma | Outcrop | Spec, XRD, XRF, AAS, ICP-MS, Petro |
| WS 08 | Lokma | Outcrop | Spec, XRD, XRF, Petro |
| WS 09 | Lokma | Outcrop | Spec |
| DC 346 | Limun | Drill core | Spec |
| DC 347 | Limun | Drill core | Spec, XRD, XRF, AAS, ICP-MS, Petro |
| DC 409 | Limun | Drill core | Spec |
| DC 350 | Lokma | Drill core | Spec |
| DC 360 | Lokma | Drill core | Spec |
| DC 361 | Lokma | Drill core | Spec, XRD, XRF, AAS, Petro |

Spec = reflectance spectroscopy; Petro = petrography; XRD = X-ray diffraction; XRF = X-ray fluorescence; AAS = atomic absorption spectrometry; ICP-MS = inductively coupled plasma mass spectrometry

Field observations included documentation of lithological boundaries, vein distribution, breccia textures, alteration halos, and structural orientations. These observations guided the sampling strategy and provided spatial context for interpreting alteration and mineralization patterns.

Sample preparation was conducted following standard homogenization protocols. Rock samples were

first air-dried and then crushed using a jaw crusher to a particle size of <2 mm. The crushed material was subjected to coning and quartering to obtain representative subsamples. These subsamples were pulverized using an agate mortar or ring mill to achieve a particle size of <75 µm (200 mesh), which is required for geochemical and mineralogical analyses. The homogenized powders were then split appropriately for use in spectroscopy, XRD, and geochemical assays.

Reflectance spectroscopy was carried out using an ASD FieldSpec4 VNIR–SWIR spectrometer, covering wavelengths from 350 to 2500 nm. Samples were measured in controlled indoor conditions under a halogen light source, with spectral data processed using continuum removal to identify characteristic absorption features of alteration minerals (Hauff, 2008; Hede et al., 2020).

Petrographic analysis was conducted on thin sections prepared from selected rock chips to observe mineral textures, alteration styles, and paragenetic sequences under a polarizing microscope. These observations provided microtextural constraints to complement spectral interpretations.

Mineral identification was further verified through XRD analysis. Each sample was pulverized to fine powder, mounted using the random powder method, and scanned from 5° to 65° 2θ at a scanning rate of 1°/min. The diffractograms were matched against standard reference patterns to confirm the presence of diagnostic alteration minerals.

Geochemical analysis included the determination of major elements by XRF, using fused-bead preparation to reduce matrix effects. Au, Ag, Zn, and Cu concentrations were determined by AAS after aqua regia digestion, which effectively mobilizes these elements from oxidized and weathered materials. For broader trace element analysis, including As, Pb, Ag, Te, Ba, and REEs, ICP-MS was employed following a 4-acid digestion ($HF–HNO_3–HClO_4–HCl$), suitable for near-total dissolution of silicate matrices.

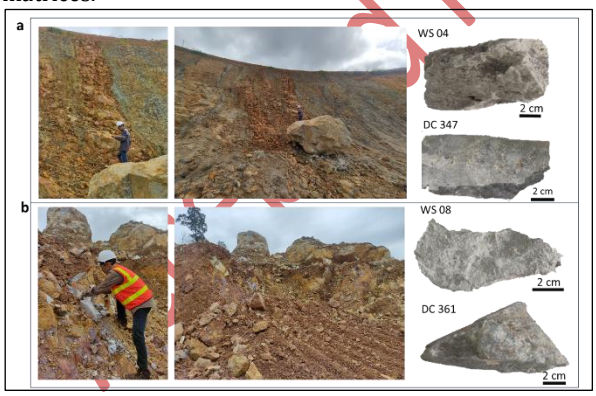


Fig. 2. Field exposures and representative hand specimens from (a) Pit Limun and (b) Pit Lokma. (a) Pit Limun: field exposures showing altered andesitic wall rocks with limonite staining and quartz–pyrite veinlets; WS 04: intensely sericitized andesite with quartz flooding and pyrite disseminations; DC 347: dark grey hydrothermal breccia with sericite–quartz–pyrite alteration and sulfide mineral indications. (b) Pit Lokma: field exposures showing intensely altered and brecciated zone with reddish-brown iron oxide-stained matrix; WS 08: pale grey, leached clay-rich rock; DC 361: pale grey crystalline tuff with quartz and supergene overprint. Scale bars = 2 cm (hand specimens only).

## 4. Results

### 4.1 Field Observations and Lithological Characteristics

Field investigations at Pit Limun and Pit Lokma identified four dominant lithological units: (1) granodioritic basement rocks of the Sukadana Batholith; (2) andesitic to dacitic volcanic flows of the Kerabai Volcanic Complex; (3) volcanic breccias and tuffs; and (4) hydrothermal breccias and quartz–sulfide vein networks.

In Pit Limun, field exposures are represented by outcrop samples WS 02, WS 03, WS 04, and WS 06, and drill core sample DC 347 (Fig. 2a). WS 02 is a dark grey andesite with hypocrystaline aphanitic texture and massive structure, preserving relict porphyritic fabric with plagioclase [phenocrysts partially replaced by sericite and disseminated pyrite in the groundmass. WS 03 is a dark grey to yellowish-brown andesite with massive structure and hypocrystaline aphanitic texture, composed primarily of hornblende [Hbl] and plagioclase [Pl] with iron oxide as a secondary mineral reflecting near-surface sulfide oxidation. WS 04 is a pale grey andesite showing intense sericitization with pervasive quartz flooding and pyrite disseminations; the relict porphyritic texture is nearly obliterated by the phyllic alteration overprint. WS 06 is a weakly altered andesite with hypocrystaline aphanitic texture and plagioclase–hornblende composition, representing the least-altered end member of the Pit Limun sample suite. Drill core sample DC 347 is a dark grey hydrothermal breccia with massive structure and hypocrystaline aphanitic texture, with indications of sulfide minerals including pyrite, chalcopyrite, and galena. Alteration in Pit Limun is dominated by phyllic-type assemblages with pervasive sericitization and localized silicification. Quartz–pyrite veins and stockworks are common, and zones of limonitization mark near-surface sulfide oxidation.

Although no large-scale discrete fault planes are directly exposed in Pit Limun, structural control is inferred from the alignment of alteration zones and mineralized corridors consistent with the regional NW–SE and NE–SW fault systems (Rustandi and De Keyser, 1993). The most direct field evidence for structural focusing is the occurrence of hydrothermal breccia bodies and quartz–pyrite vein stockworks aligned along these interpreted structural corridors, visible in field exposures.

In Pit Lokma, the geology is more complex and more intensely altered (Fig. 2b), with outcrop exposures represented by samples WS 07, WS 08, and WS 09, and drill core sample DC 361. WS 07 has hypocrystaline aphanitic texture with massive structure and advanced argillic alteration; no primary igneous texture is preserved, and the rock is composed entirely of alteration mineral assemblages. WS 08 is a grey, massive rock with hypocrystaline aphanitic texture, composed of hornblende [Hbl] and plagioclase [Pl] as primary minerals, with chalcopyrite [Ccp] as secondary mineral; advanced alteration has largely overprinted the primary fabric. WS 09 shows characteristics identical to WS 08 in terms of texture, structure, and mineral composition. Drill core sample DC 361 is a pale grey crystalline tuff with massive structure, quartz–pyrophyllite advanced argillic alteration, and evidence of supergene overprinting. Hydrothermal breccias are pervasive throughout Pit Lokma, comprising angular clasts of andesite and silicified lithologies set in a fine-grained silica–alunite–clay matrix. Breccia textures range from crackle and mosaic to jigsaw

types, with breccia bodies hosted along linear corridors aligned with the NE–SW structural trend, indicating structural control on fluid focusing. Leached, vuggy silica zones are distributed throughout Pit Lokma, representing residual silica caps formed by advanced acidic leaching.

Zones of intense alteration, brecciation, and veining are spatially concentrated along structural intersections and lithological boundaries in both pits, and these zones coincide with the highest observed gold grades as confirmed by the geochemical analysis presented in Section 4.3.

### 4.2 Alteration Mineralogy

#### 4.2.1 Reflectance Spectroscopy Analysis

Reflectance spectroscopy analysis was conducted on 15 representative rock samples collected from Pit Limun and Pit Lokma, using a spectroradiometer that covers the Visible and Near-Infrared (VNIR, 350–1100 nm) and Short-Wave Infrared (SWIR, 1100–2500 nm) regions (Fig. 3). The aim was to identify hydrothermal alteration minerals based on diagnostic absorption features and spectral shape characteristics.

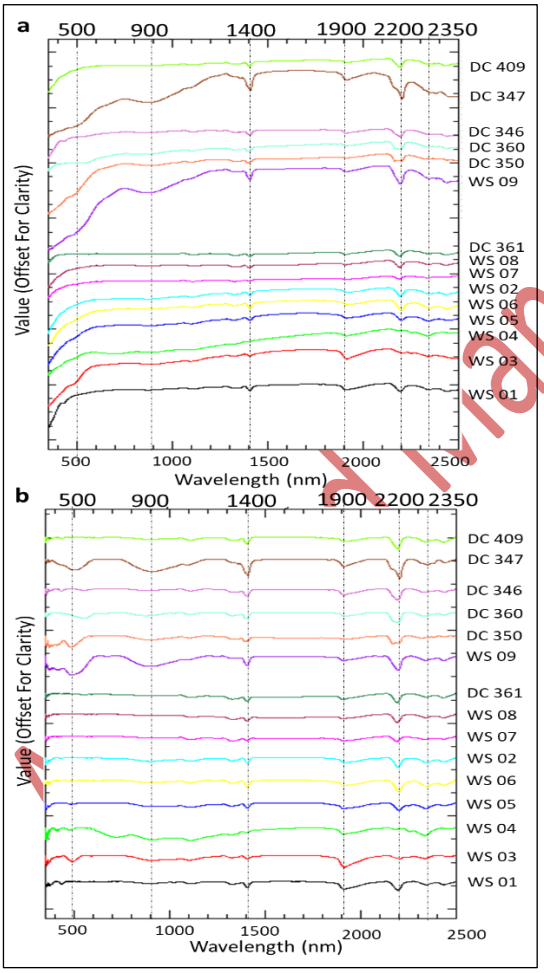


Fig 3. Reflectance spectra of all 15 rock samples from Pit Limun and Pit Lokma. (a) Raw VNIR–SWIR spectra (350–2500 nm); dashed lines mark diagnostic wavelength positions at ~500, ~900, ~1400, ~1900, ~2200, and ~2350 nm. (b) Continuum-removed spectra showing mineral identifications at key positions: ~900 nm — goethite and hematite ($Fe^{3+}$); ~1400 and ~1900 nm — OH and $H_2O$ in clay and sulfate minerals; ~2160–2170 nm — alunite (Pit Lokma); ~2200 nm — pyrophyllite and dickite; ~2205–2215 nm — illite/muscovite (Pit Limun); ~2350 nm — chlorite.

The VNIR spectral domain provides information primarily on electronic transitions of iron-bearing minerals and some organic matter. Several samples exhibited absorption features near ~430–500 nm and ~870–950 nm, associated with $Fe^{3+}$ crystal field transitions, particularly in goethite and hematite (Hauff, 2008; Hede et al., 2025). These features were commonly observed in weathered surfaces of rocks exposed near the top benches of Pit Limun and Pit Lokma, indicating near-surface oxidation of sulfide-bearing zones.

A subtle shoulder in the 650–750 nm region was noted in some spectra, interpreted as related to chlorite or residual biotite content, although these features were not well developed due to overprinting by more intense clay alteration.

The SWIR domain yielded more robust and diagnostic spectral features attributable to hydroxyl-bearing alteration minerals. The most prominent and diagnostic absorption bands were found in the 1400 nm (OH stretching), 1900 nm ($H_2O$ bending and stretching), and 2100–2250 nm regions (Al–OH and Mg–OH vibrational overtones), allowing mineralogical discrimination across the alteration zones (Hauff, 2008; Hede et al., 2018).

Samples from Pit Lokma exhibited dominant absorption features centered at:

- Alunite: sharp triplet near 2160–2170 nm, often accompanied by shoulders at ~1480 and 1730 nm.
- Dickite: absorption near 2200 nm with steep continuum slope and shoulder at ~1400 nm.
- Pyrophyllite: broader band centered near 2195–2200 nm, often overlapping with quartz background.

These features suggest intense advanced argillic alteration and sulfate mineral development, typical of high-sulfidation epithermal systems. The spectral signatures of alunite were especially well defined in matrix-supported hydrothermal breccia samples from Pit Lokma, consistent with acidic fluid alteration at high temperatures.

In contrast, samples from Pit Limun were characterized by broader and more asymmetric absorption near 2200 nm, indicative of illite and muscovite. The illite absorption centers ranged between 2195–2210 nm, with minor spectral curvature suggesting interstratified clay development. Additional minor features near 2345 nm were attributed to Mg–OH vibrations in chlorite, commonly occurring at the outer margins of the alteration zones.

The combined VNIR and SWIR analysis allowed for the preliminary classification of alteration facies based on mineral assemblages and supported the interpretation of an alteration zonation pattern progressing from quartz–illite ± chlorite (phyllic) in Pit Limun to alunite–pyrophyllite ± dickite (advanced argillic) in Pit Lokma. These results were later validated by petrographic and XRD analyses.

Additionally, the spectral data provided evidence of superimposed weathering features, particularly in samples exhibiting strong VNIR Fe-oxide signals with diminished clay absorption, suggesting post-alteration oxidative overprint. These effects were accounted for during sample interpretation.

#### 4.2.2 Petrographic Analysis

Petrographic examination of five representative thin sections from Pit Limun and Pit Lokma revealed textural and mineralogical variations consistent with distinct hydrothermal alteration styles and fluid evolution across

the two pits (Fig. 4). The observations highlight systematic differences in alteration intensity, mineral replacement sequences, and the degree of primary texture obliteration between the phyllic zone at Pit Limun and the advanced argillic zone at Pit Lokma.

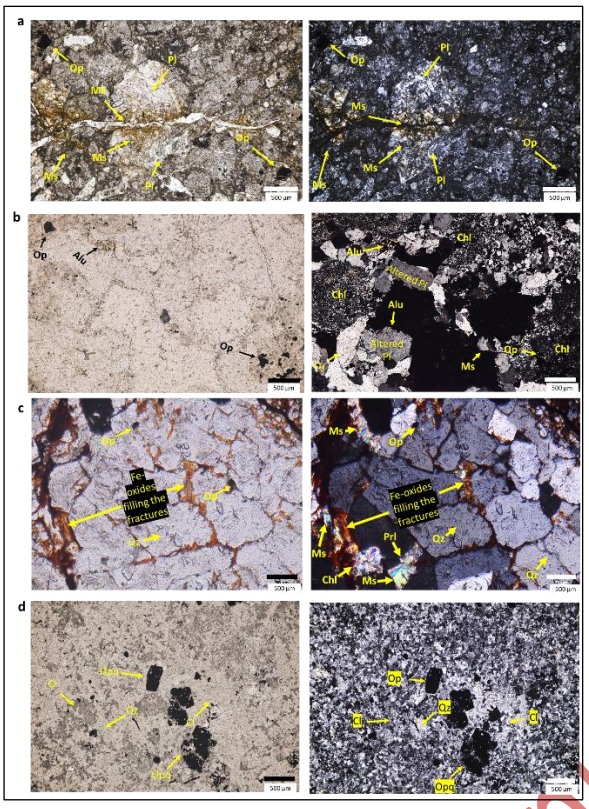


Fig 4. Representative photomicrographs of hydrothermally altered rocks from (a–b) Pit Limun and (c–d) Pit Lokma. Paired images show plane-polarized light (PPL, left) and cross-polarized light (XPL, right); scale bars = 500 µm. (a) WS 02: relict porphyritic texture with plagioclase phenocrysts partially replaced by muscovite/sericite; opaque minerals interpreted as disseminated pyrite in groundmass. (b) WS 04: intensely altered andesite; plagioclase replaced by alunite, chlorite, and sericite; disseminated opaque minerals. (c) WS 07: advanced argillic alteration with equigranular texture; assemblage of quartz, muscovite, pyrophyllite, and chlorite; no primary feldspar preserved. (d) WS 08: advanced argillic alteration with equigranular texture; quartz, fine-grained clay minerals, and opaque minerals interpreted as disseminated pyrite; no primary feldspar preserved. Mineral abbreviations: Pl — plagioclase; Ms — muscovite/sericite; Cl — clay; Alu — alunite; Chl — chlorite; Op — opaque minerals; Qz — quartz; Prl — pyrophyllite.

In Pit Limun, thin sections reveal altered andesitic rocks with varying degrees of alteration intensity, reflecting a progressive transition from moderate to intense hydrothermal overprinting. Sample WS 02 (Fig. 4a) preserves relict porphyritic texture, with plagioclase phenocrysts partially replaced by fine-grained muscovite/sericite along grain boundaries and cleavage planes, while the groundmass shows pervasive replacement by sericite and minor quartz. Biotite, where present, is altered to chlorite ± opaque minerals, indicating the breakdown of primary mafic phases under hydrothermal conditions. Opaque minerals interpreted as disseminated pyrite are observed both in the groundmass and along microfractures, commonly associated with quartz–sericite halos. The partial preservation of primary porphyritic texture and the dominance of muscovite/sericite as the feldspar replacement product are diagnostic of phyllic alteration conditions, typically formed under mildly acidic pH and intermediate temperatures of approximately 200–300 °C (Sillitoe and Hedenquist, 2003).

Sample WS 04 (Fig. 4b) represents a more intensely altered domain within Pit Limun, showing a more complex alteration assemblage that reflects higher fluid acidity. Plagioclase is altered to a skeletal texture, where the original crystal framework is preserved only as a ghost structure replaced by alunite, chlorite, and sericite, accompanied by disseminated opaque minerals. The co-occurrence of alunite alongside muscovite/sericite in WS 04 indicates a transitional zone between phyllic and advanced argillic alteration, where locally more acidic fluids have overprinted the earlier phyllic assemblage. Such overprinting textures are consistent with alteration telescoping driven by episodic fluid pulses of varying acidity, as commonly observed in high-sulfidation epithermal systems (Hedenquist et al., 2000; Einaudi et al., 2003). Quartz flooding and disseminated opaque minerals throughout the groundmass of WS 04 further support active fluid circulation under sulfidic conditions during the phyllic alteration stage.

In Pit Lokma, thin sections reveal a fundamentally different alteration style characterized by complete obliteration of primary igneous textures and pervasive replacement by advanced argillic mineral assemblages. Sample WS 07 (Fig. 4c) displays equigranular texture with no recognizable primary igneous fabric, consisting entirely of an alteration assemblage of quartz, muscovite, pyrophyllite, and chlorite with disseminated opaque minerals [Opq]. The dominance of pyrophyllite [Prl] is particularly diagnostic, as this mineral forms under high-temperature acidic conditions (>200 °C, pH <4) and is a key indicator of advanced argillic alteration in high-sulfidation epithermal systems (Myaing et al., 2018; Sillitoe and Hedenquist, 2003). The fine-grained mosaic texture of the alteration assemblage, with locally residual vugs and leached domains, reflects aggressive acid leaching by magmatic-hydrothermal fluids that dissolved and removed mobile elements including K, Na, and Ca from the host rock.

Sample WS 08 (Fig. 4d) shows a similarly intense advanced argillic alteration with equigranular texture, dominated by quartz, fine-grained clay minerals, and opaque minerals interpreted as disseminated pyrite. The clay mineral assemblage in WS 08, while appearing texturally homogeneous in thin section, cannot be individually distinguished optically and is confirmed by XRD analysis in the following subsection. The transition from the phyllic assemblage at Pit Limun to the advanced argillic assemblage at Pit Lokma records a systematic increase in fluid acidity and alteration intensity toward the interpreted core of the hydrothermal system.

### 4.2.3 XRD Analysis

X-ray diffraction (XRD) analysis was performed on six representative samples, comprising both wall outcrop and drill core materials from Pit Limun and Pit Lokma, to validate mineralogical assemblages identified through petrography and reflectance spectroscopy. The results reveal distinct mineralogical patterns corresponding to hydrothermal alteration intensity and fluid evolution in each pit.

Samples from Pit Limun (WS 01, WS 04, and DC 347) are characterized by mineral assemblages typical of phyllic alteration (Table 2). WS 01 contains abundant

quartz, muscovite, illite, and minor amounts of montmorillonite, nacrite, dickite, and gypsum, reflecting moderate alteration with supergene clay overprinting. WS 04, in addition to quartz, muscovite, and illite, contains pyrite, clinochlore, and clinopyroxene, suggesting the persistence of relict igneous phases and localized sulfide mineralization. DC 347 exhibits a similar assemblage with the addition of clintonite, jakobsite, and minor pyroxene and jarosite, indicating mixed alteration zones affected by iron enrichment and weak acid-sulfate influence.

Table 2. Identified minerals based on XRD analysis of selected samples from Pit Limun and Pit Lokma.

| Sample Code | Location | Identified Minerals |
|---|---|---|
| WS 01 | Pit Limun | quartz, muscovite,illite, montmorillonite, nacrite, dickite, gypsum |
| WS 04 | | quartz, illite, pyrite, muscovite, clinochlore, clinopyroxene, dickite, jakobsite |
| DC 347 | | quartz, illite, clintonite, muscovite, jakobsite, pyroxene, jarosite |
| WS 07 | Pit Lokma | quartz, muscovite, illite, pyrophyllite, rozenite, dickite, alunite, hollandite, andalusite, kaolinite |
| WS 08 | | quartz, muscovite, nakrite, pyrophyllite, hematite, amesite, biotite, andalusite |
| DC 361 | | quartz, birnessite, pyrophyllite, muscovite, illite, hematite, dickite, gypsum |

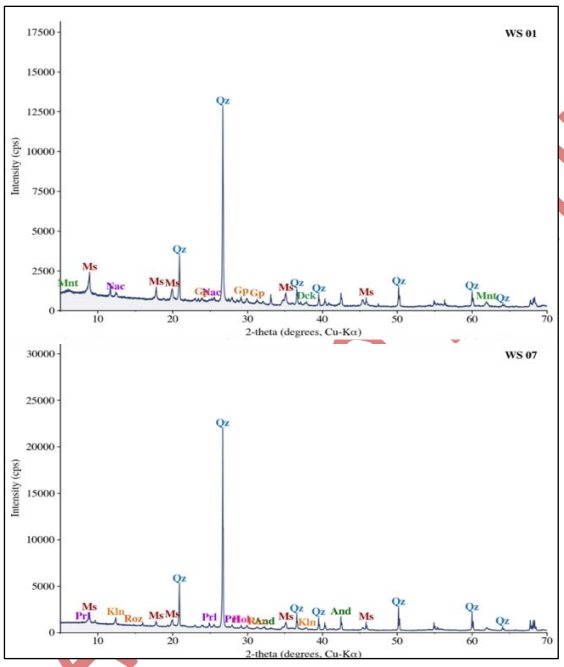


Fig 5. Representative XRD diffractograms of WS 01 from Pit Limun (top) and WS 07 from Pit Lokma (bottom). Peak labels indicate identified mineral phases based on ICDD PDF-2 reference patterns. Abbreviations: Qz = quartz; Ms = muscovite; Ilt = illite; Mnt = montmorillonite; Nac = nacrite; Dck = dickite; Gp = gypsum; Prl = pyrophyllite; Roz = rozenite; Alu = alunite; Hol = hollandite; And = andalusite; Kln = kaolinite.

In contrast, samples from Pit Lokma (WS 07, WS 08, and DC 361) exhibit mineral assemblages consistent with advanced argillic alteration. WS 07 contains a complex suite of quartz, muscovite, pyrophyllite, illite, alunite, dickite, kaolinite, and minor rozenite, hollandite, and andalusite, indicating intense acid alteration under high-temperature fluid conditions. WS 08 similarly contains quartz, muscovite, nakrite, pyrophyllite, hematite, biotite, and andalusite, suggesting deep overprinting of primary textures by acidic hydrothermal fluids. DC 361 is dominated by quartz, pyrophyllite, muscovite, and illite, with notable presence of hematite, dickite, gypsum, and birnessite, reflecting oxidative surface conditions and possible supergene enrichment.

These results confirm a clear mineralogical transition from the phyllic assemblages of Pit Limun to the advanced argillic assemblages of Pit Lokma, supporting field and petrographic evidence for a zoned high-sulfidation epithermal system. Diagnostic minerals such as pyrophyllite, alunite, dickite, and jarosite provide strong mineralogical markers for acidic hydrothermal alteration.

### 4.3 Whole-Rock Geochemistry

Whole-rock geochemical analyses were performed on selected representative samples from Pit Limun and Pit Lokma using XRF, ICP-MS, and AAS methods to determine major, trace, and precious metal concentrations. The results highlight distinct compositional trends that correspond to differences in hydrothermal alteration intensity and mineral assemblages across the two pits (Table 3).

Table 3. Whole-rock geochemical data from representative samples in Pit Limun and Pit Lokma.

XRF analysis

| Location | Pit Limun | | | Pit Lokma | | |
|---|---|---|---|---|---|---|
| Major element (%) | DC 347 | WS 01 | WS 04 | WS 08 | DC 361 | WS 07 |
| $SiO_2$ | 66.60 | 59.40 | 55.60 | 71.40 | 58.30 | 66.00 |
| $Al_2O_3$ | 22.10 | 23.50 | 22.10 | 22.10 | 27.10 | 24.60 |
| $K_2O$ | 4.91 | 5.51 | 5.00 | 1.60 | 6.29 | 4.46 |
| $Fe_2O_3$ | 3.36 | 4.00 | 5.55 | 3.23 | 2.93 | 3.56 |
| Na2O | 0.54 | 0.17 | 0.22 | 0.26 | 0.34 | 0.24 |
| $TiO_2$ | 0.43 | 0.70 | 0.79 | 0.50 | 0.79 | 0.62 |
| $P_2O_5$ | 0.50 | 0.35 | 0.53 | 0.17 | 0.60 | 0.12 |
| $SO_3$ | 0.34 | 4.22 | 4.19 | 0.34 | 2.28 | 0.14 |
| Cl | 0.21 | 0.20 | 0.05 | 0.22 | 0.11 | 0.12 |
| MgO | 0.03 | 1.22 | 4.68 | nd | 0.10 | 0.04 |
| MnO | 0.02 | 0.03 | 0.19 | nd | nd | nd |

nd = not detected

ICP-MS analysis

| Sample | DC 347 | WS 07 | Sample | DC 347 | WS 07 |
|---|---|---|---|---|---|
| Trace element | Content (ppm) | | Trace element | Content (ppm) | |
| Ca | 3,316.71 | 386.25 | Y | 4.52 | 7.36 |
| Pb | 934.41 | 51.50 | Te | 8.39 | 0.42 |
| Ag | 29.43 | 0.82 | La | 23.81 | 27.71 |
| B | 258.21 | 127.24 | Ce | 51.10 | 57.81 |
| V | 83.79 | 83.68 | Pr | 0.53 | 5.18 |
| Cr | 19.09 | 15.24 | Nd | 1.99 | 19.58 |
| Mn | 70.36 | 24.61 | Sm | 3.46 | 4.42 |
| Co | 9.76 | 2.00 | Eu | 1.20 | 1.26 |
| Ni | 5.18 | 7.30 | Gd | 3.33 | 3.97 |
| Ga | 32.94 | 16.84 | Dy | 1.27 | 1.91 |
| As | 63.47 | 32.97 | Ho | 0.22 | 0.36 |
| Se | 8.71 | 1.06 | Er | 0.66 | 0.94 |
| Rb | 66.54 | 125.04 | Tm | 0.10 | 0.14 |
| Sr | 292.82 | 228.40 | Yb | 0.71 | 0.78 |
| Mo | 3.56 | 7.03 | Ti | 0.42 | 0.53 |
| Cd | 2.20 | 0.17 | U | 2.32 | 2.54 |
| Ba | 928.10 | 571.90 | Li | <0.0001 | 2.0834 |
| | | | Be | <0.0001 | <0.0001 |

AAS analysis

| Sample | Content (%, except Au in ppm) | | | |
|---|---|---|---|---|
| | Au | Ag | Zn | Cu |
| WS 04 | 0.09 | 0.5 | 0.003 | 0.0052 |
| WS 07 | 0.05 | 0.5 | 3E-04 | 0.0008 |
| WS 03 | 0.59 | 0.5 | 0.011 | 0.003 |
| DC 347 | 1.61 | 0.5 | 0.004 | 0,0032 |
| DC 361 | 0.53 | 0.5 | 3E-04 | 0,0006 |

XRF analysis reveals that the silica content ($SiO_2$) varies widely from 55.60 to 71.40 wt.%, with the highest values observed in sample WS 08 from Pit Lokma, consistent with intense silicification. $Al_2O_3$ contents range from 22.10 to 27.10 wt.%, with elevated values in Pit Lokma samples (e.g., DC 361), suggesting the development of advanced clay-rich assemblages. $K_2O$

contents are relatively high in several Pit Limun samples (up to 5.51 wt.% in WS 01), indicating the presence of K-bearing phases such as muscovite and illite. In contrast, Pit Lokma samples show systematically low MgO and MnO concentrations, with MgO <0.1 wt.% and MnO below detection limits in samples WS 07, WS 08, and DC 361, consistent with pervasive dissolution of primary Mg–Mn-bearing phases such as biotite and hornblende by acidic hydrothermal fluids during advanced argillic alteration. This interpretation is supported by the absence of biotite and hornblende in the XRD patterns of all Pit Lokma samples (Table 2), in contrast to their presence in phyllic-zone samples WS 04 and DC 347.

ICP-MS analyses of selected drill core and surface samples (e.g., DC 347 from Pit Limun and WS 07 from Pit Lokma) indicate contrasting trace element distributions. Notably, DC 347 exhibits significantly elevated concentrations of Pb (934 ppm), Ag (29.4 ppm), and Ba (928 ppm), which are substantially higher than those in WS 07 (Pb: 51.5 ppm, Ag: 0.82 ppm, Ba: 572 ppm). This suggests a stronger association of base and precious metals with the alteration zones in Pit Limun.

Rare earth elements (REEs), including light REEs such as La, Ce, and Nd, are enriched in both samples but notably higher in WS 07, with Ce reaching 57.8 ppm and Nd up to 19.6 ppm. This enrichment pattern is consistent with high-temperature acidic alteration, potentially reflecting REE mobilization and fixation during advanced argillic alteration.

AAS analyses confirm the presence of gold (Au) in both pits, with sample DC 347 (Pit Limun) showing the highest concentration (1.61 ppm), whereas other samples contain Au in the range of 0.05 to 0.59 ppm. The Cu and Zn contents are generally low across all samples, although slightly elevated Zn values (0.0112 wt.%) are found in WS 03. These results suggest that gold mineralization is primarily associated with hydrothermal activity in Pit Limun, potentially linked to quartz–pyrite vein systems and sericite-rich alteration halos.

## 5. Discussion

### 5.1 Hydrothermal Alteration Zonation

The hydrothermal alteration patterns at Pit Limun and Pit Lokma display a well-defined spatial zonation characteristic of HS epithermal systems. The integration of mineralogical, spectral, petrographic, and geochemical data reveals two dominant alteration regimes: an advanced argillic zone at Pit Lokma and a phyllic zone at Pit Limun.

The advanced argillic assemblage at Pit Lokma, dominated by alunite, pyrophyllite, and dickite with vuggy silica, is consistent with hypogene magmatic-hydrothermal condensation in a lithocap environment, as distinct from steam-heated or supergene advanced argillic assemblages (Hedenquist and Arribas, 2022). SWIR spectra display prominent absorption near 2.17–2.20 μm (Al–OH bond), consistent with kaolinite-group and alunite-group minerals. Vuggy silica textures and leached breccia matrices confirmed by petrography indicate aggressive acidic fluid interaction, resulting in the removal of mobile elements (K, Na, Ca) and the preservation of immobile quartz and aluminosilicates (Dubé et al., 1998; Espi et al., 2002; Sillitoe and Hedenquist, 2003)

Pit Limun is dominated by phyllic alteration, characterized by the pervasive replacement of plagioclase and K-feldspar phenocrysts and groundmass by muscovite/sericite and quartz, with accessory chlorite and pyrite, confirmed by petrography, XRD, and the characteristic Al–OH absorption at ~2.20 μm.

The classification of Pit Limun alteration as phyllic rather than argillic is based on three lines of evidence. First, XRD analysis of all Pit Limun samples (WS 01, WS 04, DC 347) shows that muscovite and illite are the dominant clay-bearing phases, with smectite and kaolinite occurring only as minor accessory minerals and not as primary feldspar replacement products. In argillic alteration, smectite, kaolinite, or halloysite would dominate the assemblage as the principal products of feldspar breakdown. Second, petrographic analysis of samples WS 02, WS 04, and DC 347 confirms that plagioclase phenocrysts and groundmass are pervasively replaced by fine-grained sericite/muscovite, a texture diagnostic of phyllic conditions, contrasting with argillic alteration where feldspar replacement by smectite or kaolinite produces a fine-grained clay texture without the silky micaceous character of sericite. Third, disseminated pyrite and pervasive quartz flooding co-occur throughout the groundmass of all Pit Limun samples, consistent with moderately acidic, sulfidic fluid conditions at 200–300 °C that define the phyllic facies (Pirajno, 2009; Sillitoe and Hedenquist, 2003), contrasting with argillic alteration formed at lower temperatures (<150 °C) under near-neutral to weakly acidic pH where pyrite and quartz flooding are less pervasive.

Phyllic alteration may develop during both prograde hydrothermal activity and retrograde waning of the system. The presence of jarosite in DC 347 is consistent with retrograde oxidation of pyrite by residual acid-sulfate fluids during system waning, a process well documented in the late-stage evolution of magmatic-hydrothermal epithermal systems (Rye, 2005). Mixed-assemblage breccia clasts preserving relict sericite within an otherwise advanced argillic matrix record overprinting by successive fluid pulses, consistent with alteration telescoping under episodic depressurization (Hedenquist et al., 2000; Einaudi et al., 2003).

Although propylitic alteration is commonly developed at the peripheral or deeper levels of epithermal systems, no clear evidence of propylitic assemblages (e.g., epidote, actinolite, abundant chlorite ± calcite) was identified in either Pit Limun or Pit Lokma. Chlorite and minor clinopyroxene were detected in WS 04 and DC 347 (Pit Limun) based on XRD, but these occur as accessory minerals and are more likely relics of weak retrograde metamorphism or background alteration in the host rocks rather than a developed propylitic halo.

The absence of a distinct propylitic zone in this study area may reflect the limited lateral and vertical exposure, and/or an erosion level that has removed these outer zones. It may also indicate that hydrothermal fluids were predominantly acidic and structurally focused, thereby restricting the development of neutral-to-weakly alkaline fluid regimes needed for typical propylitic alteration. This spatial restriction is typical of telescope systems where advanced argillic and phyllic zones are superimposed directly onto the host volcanic rocks.

Furthermore, the spatial juxtaposition of phyllic and advanced argillic zones implies a lateral as well as vertical component of fluid flow, likely controlled by intersecting fault systems. The lateral extent of advanced argillic alteration overlying or adjacent to phyllic zones suggests that acidic vapor-dominated fluids migrated both upward

and outward from the central conduit zone, with decreasing temperature and increasing pH favoring the stability of sericite-bearing assemblages at depth.

The alteration zonation from Pit Lokma to Pit Limun records the evolution of hydrothermal fluids and physicochemical gradients within the epithermal system. This zonation not only reflects the degree of fluid–rock interaction and host-rock susceptibility but also provides key vectors for exploration targeting in similar high-sulfidation environments.

### 5.2 Characterization and Controls on Mineralization

The mineralization in the study area is closely associated with distinct hydrothermal alteration styles and structurally controlled fluid pathways. Integration of geochemical, mineralogical, and petrographic data reveals two geochemically and mineralogically contrasting environments: a moderately mineralized phyllic zone in Pit Limun and a strongly altered, but weakly mineralized, advanced argillic zone in Pit Lokma.

In Pit Limun, the occurrence of gold mineralization is spatially correlated with zones of quartz–sericite–pyrite alteration, as evidenced by Au concentrations reaching up to 1.61 ppm (DC 347), accompanied by elevated Ag, Pb, and Zn values from AAS and ICP-MS analyses. Thin section observations confirm pervasive sericitization of plagioclase and fine-grained quartz flooding in the groundmass, while pyrite occurs as disseminations and veinlet infillings. The XRF data also show elevated $K_2O$ and $Fe_2O_3$ concentrations, supporting the abundance of sericite and pyrite, both of which are common hosts and pathfinders for gold in high-sulfidation systems. This alteration–mineralization relationship suggests that Pit Limun represents a favorable depositional environment for Au-bearing fluids, potentially located near the base or margins of a hydrothermal conduit.

In contrast, Pit Lokma is characterized by residual silica, advanced argillic minerals (alunite, pyrophyllite, dickite), and exhibits strong leaching of mobile elements, including K, Na, and Ca. The low $K_2O$ values (<2%) and near-complete absence of feldspar phases indicate extensive alteration under acidic conditions, likely in a vapor-dominated regime. Despite intense alteration, Au concentrations in this zone are low (e.g., WS 07: 0.05 ppm), consistent with fluid pathways that bypassed depositional traps or zones of metal fixation. The trace element patterns support this: samples from Pit Lokma exhibit lower concentrations of Ag, Pb, and Zn, while showing enrichments in rare earth elements (e.g., Ce, Nd) and sulfate-related phases such as jarosite and rozenite, indicative of oxidizing, acidic, and possibly reworked conditions.

The structural architecture plays a central role in controlling fluid flow and localization of alteration and mineralization. Field observations and satellite imagery show that hydrothermal breccias, vuggy silica zones, and quartz–pyrite veins align with NW–SE and NE–SW fault systems. These intersecting structures likely acted as permeable conduits for hydrothermal fluids, promoting vertical fluid migration and lateral dispersion. The presence of jigsaw-textured breccias with a silica–alunite matrix supports episodic pressurization and hydrofracturing processes that can enhance permeability and facilitate the transport and local deposition of metal-bearing fluids.

Pathfinder element associations provide further insight into the geochemical evolution of the hydrothermal system. The gold-bearing sample DC 347 from Pit Limun shows elevated As (63.47 ppm) and Pb (934 ppm) relative to WS 07 from Pit Lokma (As: 32.97 ppm; Pb: 51.50 ppm), consistent with metal transport and deposition in the phyllic zone. In contrast, WS 07 shows enrichment in REEs and sulfate phases, indicating advanced leaching and fluid neutralization with minimal metal deposition (Tun et al., 2019).

These patterns indicate a zoned hydrothermal system, with advanced argillic alteration and leaching predominating in the upper zones (Pit Lokma), transitioning downward into more reduced, structurally focused zones of mineralization (Pit Limun). The data support a model of fluid ascent through structurally controlled pathways, with telescoped alteration assemblages resulting from multiple fluid pulses under fluctuating pressure-temperature-chemical regimes.

The combination of quartz–sericite alteration, pyrite dissemination, elevated pathfinder elements, and structural focusing in Pit Limun defines it as a key mineralized zone within this system. Meanwhile, Pit Lokma represents a hydrothermally overprinted discharge zone, where intense leaching has removed or prevented metal accumulation. Future exploration should prioritize depth extensions and structural intersections beneath Pit Lokma, as well as along the transitional corridors between the two pits.

### 5.3 Classification and Genetic Model of the Deposits

Based on the integration of field observations, petrographic analysis, mineralogical assemblages, geochemical data, and alteration zonation, the mineralization styles in the Limun and Lokma Pits are best classified as part of a high-sulfidation epithermal system. Several converging lines of evidence support this classification.

The observed alteration and mineralization characteristics are consistent with the high-sulfidation epithermal model (Sillitoe, 2010; Sillitoe and Hedenquist, 2003; White and Hedenquist, 1995). Comparable HSE systems in Indonesia, including the Tumpangpitu deposit in East Java, have been documented with similar assemblages of alunite, pyrophyllite, and advanced argillic alteration (Myaing et al., 2018).

High-sulfidation systems typically form in volcanic or subvolcanic settings under oxidized, acidic conditions resulting from the condensation of magmatic volatiles. The hallmark features observed in this study include:

- Advanced argillic alteration at Pit Lokma, dominated by alunite, dickite, pyrophyllite, and quartz, is indicative of a highly acidic and oxidized hydrothermal fluid overprint.
- Phyllic alteration (sericitic) at Pit Limun, characterized by pervasive sericitization of feldspars and the groundmass, and presence of disseminated pyrite ± quartz veinlets.
- Textural evidence such as vuggy silica, brecciation, and massive silicification zones.
- Geochemical signature of elevated Au associated with enrichment in As, Pb, and Te in the gold-bearing phyllic zone (DC 347).

These characteristics align with the upper portions of a high-sulfidation system, typically representing the upflow zones near or within the lithocap.

Table 4. Paragenetic sequence of minerals based on integrated field, petrographic, and XRD data. Symbol key: ■ = active precipitation interval during the indicated stage; ↓ = replacement/destruction of primary mineral phase by hydrothermal processes.

| Mineral | Stage 1 (host rock) | Stage IIa (Prograde Alteration) | Stage IIb (retrograde/ waning) | Stage III (Ore Mineralization) | Stage IV (supergene oxidation) |
|---|---|---|---|---|---|
| Plagioclase | ■■■■ | ↓ | | | |
| Hornblende / Biotite | ■■■■ | ↓ | | | |
| Primary Quartz | ■■■ | | | | |
| Vuggy Quartz | | ■■■■■■ | | | |
| Hydrothermal Quartz | | | ■■■■■■ | ■■■■■ | |
| Alunite | | ■■■■■■ | ■■ | | |
| Pyrophyllite | | ■■■■■ | | | |
| Andalusite | | ■■ | | | |
| Dickite | | ■■■■ | ■■■■ | | |
| Muscovite / Sericite | | ■■■■ | ■■■■■■ | ■■ | |
| Kaolinite / Clays | | | ■■■■ | ■■ | ■■ |
| Pyrite | | ■■ | ■■■■■■ | ■■■■■ | ↓ |
| Jarosite | | | ■■ | | ■■■■ |
| Fe-Oxides (Goethite) | | | | | ■■■■■■ |
| Gypsum | | | | | ■■■■ |

The paragenetic relationship (Table 4) and alteration assemblages indicate a vertical zonation of the hydrothermal system consistent with the classical high-sulfidation epithermal model (Sillitoe and Hedenquist, 2003). The upper zone, represented by Pit Lokma, is characterized by advanced argillic alteration (Stage IIa) including vuggy silica, alunite, pyrophyllite, dickite, and residual quartz, associated with elevated As and Te concentrations, light REE enrichment, and Fe-oxide cementation in fractures. The intermediate zone, represented by Pit Limun, is dominated by phyllic alteration with muscovite/sericite, illite, chlorite, and disseminated pyrite ± quartz veinlets, spatially associated with the highest gold concentrations recorded in this study. Phyllic alteration persists into Stage IIb (retrograde/waning), where the presence of jarosite in sample DC 347 records retrograde acid-sulfate oxidation of pyrite during system waning. Peripheral propylitic zones dominated by chlorite ± epidot are inferred but not directly confirmed by sampling. The supergene stage (Stage III) is marked by goethite/limonite formed by oxidation of pyrite under surface weathering conditions, consistent with the iron-stained limonitization observed in field exposures (Fig. 2).

Regarding ore minerals, gold, chalcopyrite, and telluride minerals are not included in Table 3 as none of these phases were identified as discrete mineral phases by XRD or petrographic analysis. Gold is detected only geochemically by AAS, it is interpreted as occurring as submicroscopic inclusions within pyrite, co-precipitated with the phyllic alteration assemblage, consistent with its spatial association with quartz–sericite–pyrite zones. The possible presence of chalcopyrite is inferred from megascopic observations of sulfide minerals in DC 347 and elevated Cu concentrations in AAS data, while telluride minerals are inferred from elevated Te concentrations from ICP-MS data. Neither chalcopyrite nor telluride minerals were confirmed by XRD or petrographic analysis; their direct identification would require higher-resolution analytical methods, which are recommended for future work.

This alteration zonation is consistent with the classical high-sulfidation model, where a steam-heated, acidic lithocap is underlain by zones of quartz–alunite and quartz–sericite–pyrite, overprinting earlier propylitic assemblages (Sillitoe and Hedenquist, 2003).

The genetic evolution of the deposit likely involved multiple overprinting hydrothermal events. Initially, magmatic fluids exsolved from an underlying intrusion migrated upward, becoming increasingly acidic through condensation and fluid–rock interaction. These fluids cause leaching and the formation of residual quartz in the uppermost zones (Pit Lokma), with widespread precipitation of alunite and clay minerals during fluid neutralization. As the system entered a retrograde, waning stage (Stage IIb), cooler, less acidic fluids continued to precipitate muscovite/sericite, while oxidation of pyrite produced jarosite in DC 347, indicating a transition toward supergene conditions.

The hydrothermal breccia textures preserved alteration relicts within breccia clasts, and sharp clast–matrix boundaries further indicate episodic pressure fluctuations and boiling, potentially driven by magma depressurization or fault-valve behavior. These mechanisms are key drivers in vertical metal zoning and rapid mineral precipitation in high-sulfidation environments.

## 6. Conclusions

This study integrates geological, mineralogical, and geochemical analyses to characterize the nature, zonation, and genesis of high-sulfidation epithermal mineralization at Pit Limun and Pit Lokma, Ketapang Regency, West Kalimantan. The conclusions are summarized as follows:

- Field observations, petrographic analysis, and XRD data reveal a well-developed alteration zonation typical of high-sulfidation epithermal systems. The alteration is dominated by advanced argillic zones characterized by quartz, alunite, pyrophyllite, kaolinite, and dickite; intermediate argillic zones dominated by sericite and illite; and subordinate propylitic assemblages inferred at depth, with chlorite occurring as an accessory phase in phyllic-zone samples. Vuggy silica textures and residual quartz zones mark the more intensely leached cores.
- Whole-rock geochemistry (XRF, ICP-MS, AAS) highlights enrichment of $SiO_2$, $Al_2O_3$, and trace elements such as As, Se, and Pb within altered zones, correlating with pyrite and minor Au contents. Elevated rare earth elements (REEs), including Ce, Nd, and La, are associated with advanced alteration, suggesting the mobility of light REEs during acidic

hydrothermal fluid interaction. Gold mineralization is closely associated with phyllic alteration zones and the presence of pyrite with elevated As concentrations providing a geochemical vector toward mineralized intervals.

- Structural control by NW–SE and NE–SW trending fault systems is inferred from both the alignment of hydrothermal breccia bodies, quartz–sulfide veins, and alteration zones documented in field exposures, and from the regional structural framework of West Kalimantan. The highest gold concentrations and most intense alteration are spatially concentrated along these interpreted structural corridors, supporting their role as primary conduits for hydrothermal fluid migration.
- The integrated paragenetic sequence supports classification of the system as a high-sulfidation epithermal deposit, genetically linked to shallow-level magmatic intrusions of the Kerabai Volcanic Complex.

**Acknowledgements**

This research was financially supported by the Research, Community Service, and Innovation (Penelitian, Pengabdian Masyarakat, dan Inovasi – PPMI) scheme of Institut Teknologi Bandung for the year 2024.

**References**

Angeles, C.A., Prihatmoko, S., Walker, J.S., 2002. Geology and Alteration-Mineralization Characteristics of the Cibaliung Epithermal Gold Deposit, Banten, Indonesia. Resource Geology 52. https://doi.org/10.1111/j.1751-3928.2002.tb00143.x

Carlile, J.C., Mitchell, A.H.G., 1994. Magmatic arcs and associated gold and copper mineralization in Indonesia. J. Geochem. Explor. 50, 91–142. https://doi.org/10.1016/0375-6742(94)90022-1

Dubé, B., Dunning, G., Lauzière, K., 1998. Geology of the Hope Brook Mine, Newfoundland, Canada: a preserved late Proterozoic high-sulfidation epithermal gold deposit and its implications for exploration. Economic Geology 93. https://doi.org/10.2113/gsecongeo.93.4.405

Ernawati, R., Idrus, A., Tri, H., Petrus, B.M., 2019. Mineralogy and Geochemistry of Gold Ore Low Sulfidation -Epithermal at Lamuntet, Brang Rea, West Sumbawa District, West Nusa Tenggara Province. Journal of Geoscience, Engineering, Environment, and Technology 4, 198–207. https://doi.org/10.25299/JGEET.2019.4.3.1653

Espi, J.O., Kajiwara, Y., Hawkins, M.A., Bainbridge, T., 2002. Hydrothermal Alteration and Cu-Au Mineralization at Nena High Sulfidation-type Deposit, Frieda River, Papua New Guinea. Resource Geology 52. https://doi.org/10.1111/j.1751-3928.2002.tb00141.x

Gemmell, J.B., 2007. Hydrothermal alteration associated with the Gosowong epithermal Au-Ag deposit, Halmahera, Indonesia: Mineralogy, geochemistry, and exploration implications. Economic Geology 102. https://doi.org/10.2113/gsecongeo.102.5.893

Hall, R., 2012. Late Jurassic–Cenozoic reconstructions of the Indonesian region and the Indian Ocean. Tectonophysics 570–571, 1–41. https://doi.org/https://doi.org/10.1016/j.tecto.2012.04.021

Hall, R., 2002. Cenozoic geological and plate tectonic evolution of SE Asia and the SW Pacific: computer-based reconstructions, model and animations. J. Asian Earth Sci. 20, 353–431. https://doi.org/10.1016/S1367-9120(01)00069-4

Hasria, H., Idrus, A., Warmada, I.W., 2019. Alteration Alteration, Mineralization and Geochemistry of Metamorphic Rocks Hosted Hydrothermal Gold Deposit at Rumbia Mountains, Bombana Regency, Southeast Sulawesi, Indonesia. Journal of Geoscience, Engineering, Environment, and Technology 4. https://doi.org/10.25299/jgeet.2019.4.2.2346

Hauff, P.L., 2008. An overview of VIS-NIR-SWIR field spectroscopy as applied to precious metals exploration, Hauff, Phoebe. Arvada, Colorado.

Hede, A.N.H., Heriawan, M.N., Syafrizal, S., 2020. Pemanfaatan spektroskopi reflektansi dalam pengindraan jauh sensor optis untuk eksplorasi mineral. Prosiding Temu Profesi Tahunan PERHAPI; 2020: PROSIDING TEMU PROFESI TAHUNAN PERHAPIDO - 10.36986/ptptp.v0i0.1311–12.

Hede, A.N.H., Kusuma, G.J., Maghfira, S., Badhuraman, A., Sakti, A.D., 2025. Characterizing acid mine drainage in coal mine sumps using reflectance spectroscopy and PlanetScope SuperDove imagery. Earth Sci. Inform. 18, 1–18. https://doi.org/10.1007/S12145-025-01826-9/METRICS

Hede, A.N.H., Syafrizal, Gunawan, S., 2018. Assessment of granitoid-related mineralization using visible near-infrared and shortwave infrared reflectance spectroscopy, in: International Symposium on Earth Science and Technology 2018. pp. 144–149.

Hedenquist, J.W., Arribas, A., 2022. Exploration Implications of Multiple Formation Environments of Advanced Argillic Minerals. Economic Geology 117. https://doi.org/10.5382/econgeo.4880

Hedenquist, J.W., Arribas, A., Gonzalez-Urien, E., 2000. Exploration for epithermal gold deposits, in: Hagemann, S.G., Brown, P.E. (Eds.), . Society of Economic Geologist.

Heriawan, M.N., Hafizh, A., Suryantini, Hede, A.N.H., Iskandar, C., 2022. Surface Lineament Density and Its Correlation with the Subsurface Permeable Zones at Patuha Geothermal Field, West Java, Indonesia, in: Advances in Science, Technology and Innovation. https://doi.org/10.1007/978-3-030-72896-0_64

Idrus, A., Prihatmoko, S., Harjanto, E., Meyer, F.M., Nur, I., Widodo, W., Agung, L.N., 2017. Metamorphic rock-hosted orogenic gold deposit style at Bombana (Southeast Sulawesi) and Buru Island (Maluku): Their key features and significances for gold exploration in Eastern Indonesia. Journal of Geoscience, Engineering, Environment, and Technology 2. https://doi.org/10.24273/jgeet.2017.2.2.291

Idrus, A., Ubaidillah, A.S., Warmada, I.W., Maula, S., 2021. Geology, Rock Geochemistry and Ore Fluid Characteristics of the Brambang Copper-Gold Porphyry Prospect, Lombok Island, Indonesia. Journal of Geoscience, Engineering, Environment, and Technology 6. https://doi.org/10.25299/jgeet.2021.6.1.6145

Ilmawan, I., Idrus, A., Lai, C.K., Dana, C.D.P., Nugroho, A.P.A., 2023. Intermediate-sulfidation epithermal mineralization at Monterado goldfield in Western Borneo (Indonesia): Geological, mineralogical, and fluid inclusion microthermometric perspectives. Geological Journal 58, 315–332. https://doi.org/10.1002/GJ.4594

Myaing, Y.Y., Idrus, A., Titisari, A.D., 2018. Fluid Inclusion Study of The Tumpangpitu High Sulfidation Epithermal Gold Deposit in Banyuwangi District, East Java, Indonesia. Journal of Geoscience, Engineering, Environment, and Technology 3. https://doi.org/10.24273/jgeet.2018.3.01.1039

Pirajno, F., 2009. Hydrothermal Processes and Wall Rock Alteration BT - Hydrothermal Processes and Mineral Systems, in: Pirajno, F. (Ed.), . Springer Netherlands, Dordrecht, pp. 73–164. https://doi.org/10.1007/978-1-4020-8613-7_2

Prihatmoko, S., Idrus, A., 2020. Low-sulfidation epithermal gold deposits in Java, Indonesia: Characteristics and linkage to the volcano-tectonic setting. Ore Geol. Rev. 121. https://doi.org/10.1016/J.OREGEOREV.2020.103490

Rustandi, E., De Keyser, F., 1993. Geological map of the Ketapang sheet, Kalimantan. Bandung.

Rye, R.O., 2005. A review of the stable-isotope geochemistry of sulfate minerals in selected igneous environments and related hydrothermal systems. Chem. Geol. 215. https://doi.org/10.1016/j.chemgeo.2004.06.034

Sillitoe, R.H., 2010. Porphyry Copper Systems. Economic Geology 105, 3–41. https://doi.org/10.2113/GSECONGEO.105.1.3

Sillitoe, R.H., Hedenquist, J.W., 2003. Linkages between Volcanotectonic Settings, Ore-Fluid Compositions, and Epithermal Precious Metal Deposits, in: Simmons, S.F., Graham, I. (Eds.), Volcanic, Geothermal, and Ore-Forming Fluids: Rulers and Witnesses of Processes within the Earth. Society of Economic Geologists, pp. 315–343.

Syafrizal, Rivai, T.A., Yonezu, K., Kusumanto, D., Watanabe, K., Hede, A.N.H., 2017. Characteristics of a low-sulfidation epithermal deposit in the River Reef Zone and the Watuputih Hill, the Poboya gold prospect, Central Sulawesi, Indonesia: Host rocks and hydrothermal alteration. Minerals 7. https://doi.org/10.3390/min7070124

Tun, M.M., Warmada, I.W., Idrus, A., Harijoko, A., Yonezu, K., Watanabe, K., Tun, M.M., Warmada, I.W., Idrus, A., Harijoko, A., Yonezu, K., Watanabe, K., 2019. Geochemical Behavior of Trace- and Rare-Earth Elements in the Hydrothermal Alteration Facies of the Cijulang Area, West Java, Indonesia. Open Journal of Geology 9, 278–294. https://doi.org/10.4236/OJG.2019.95019

White, N.C., Hedenquist, J.W., 1995. Epithermal Gold Deposits: Styles, Characteristics and Exploration. SEG Discovery 1–13. https://doi.org/10.5382/SEGnews.1995-23.fea

Williams, P.R., Johnston, C.R., Almond, R.A., Simamora, W.H., 1988. Late cretaceous to early tertiary structural elements of west Kalimantan. Tectonophysics 148. https://doi.org/10.1016/0040-1951(88)90135-7

Williams, P.R., Supriatna, S., Harahap, B., 1986. Cretaceous mélange in West Kalimantan and its tectonic implications. Bulletin of the Geological Society of Malaysia 19, 69–78. https://doi.org/10.7186/BGSM19198606